



Confronting the water potential information gap

Kimberly A. Novick¹✉, Darren L. Ficklin², Dennis Baldocchi³, Kenneth J. Davis⁴,
Teamrat A. Ghezzehei⁵, Alexandra G. Konings⁶, Natasha MacBean², Nina Raoult⁷,
Russell L. Scott⁸, Yuning Shi⁹, Benjamin N. Sulman¹⁰ and Jeffrey D. Wood¹¹

Water potential directly controls the function of leaves, roots and microbes, and gradients in water potential drive water flows throughout the soil–plant–atmosphere continuum. Notwithstanding its clear relevance for many ecosystem processes, soil water potential is rarely measured in situ, and plant water potential observations are generally discrete, sparse, and not yet aggregated into accessible databases. These gaps limit our conceptual understanding of biophysical responses to moisture stress and inject large uncertainty into hydrologic and land-surface models. Here, we outline the conceptual and predictive gains that could be made with more continuous and discoverable observations of water potential in soils and plants. We discuss improvements to sensor technologies that facilitate in situ characterization of water potential, as well as strategies for building new networks that aggregate water potential data across sites. We end by highlighting novel opportunities for linking more representative site-level observations of water potential to remotely sensed proxies. Together, these considerations offer a road map for clearer links between ecohydrological processes and the water potential gradients that have the ‘potential’ to substantially reduce conceptual and modelling uncertainties.

Gradients in the water potential (Ψ) of soils and plants form the energetic basis for the transport of water, and elements contained therein, through a connected continuum linking the deepest soil layers to the top of plant canopies (Fig. 1). The Ψ can be a positive or negative pressure, although it is typically negative—a tension force—in unsaturated soils and within plant hydraulic systems. Ψ gradients have been recognized as the fundamental driver of water fluxes between soils, streams and groundwater for more than a century, and they appear in some of the most foundational equations in hydrology¹ (for example, Darcy’s Law and Richards’ Equation). Likewise, the critical role of Ψ gradients in driving water flows through the soil–plant–atmosphere continuum has been known for decades².

Beyond redistributing water through ecosystems, Ψ is also a direct control of many biophysical processes. Soil Ψ (Ψ_s) regulates the flow of water into and out of soil microbe cells and determines their metabolism³. In plants, leaf Ψ (Ψ_l) is a key driver of stomatal conductance and photosynthetic carbon uptake^{4,5}, and its close connection to branch and stem Ψ (Ψ_x) controls the risk of drought-driven xylem embolism and mortality^{6,7}. Consequently, most ecosystem services, including water storage, food and fibre supply, and water and climate regulation, are fundamentally linked to Ψ .

While undeniably important for soil and plant function, for reasons that will be discussed in more detail, Ψ_s is rarely measured in situ^{8,9}, and observations of plant Ψ have historically been limited to destructive and disjunct manual measurements. The objective of this paper is to demonstrate key uncertainties linked to the dearth of soil and plant Ψ data and to discuss the theoretical and modelling progress that could be enabled with richer and more discoverable

information about Ψ . We begin by discussing issues surrounding the measurement, modelling and synthesis of Ψ_s and then address additional considerations linked to the measurement and prediction of Ψ in plants. We then present a road map for creating accessible and open Ψ databases and discuss promising new approaches for detecting Ψ using remote sensing.

Concepts and uncertainties linked to Ψ_s

Water flows ‘downhill’ energetically, moving from areas of higher potential to areas of lower potential, such that Ψ_s gradients are the driving force of subsurface water flows¹. In most unsaturated soils, Ψ_s is dominated by the matric potential, which becomes more negative when soils dry, and the effective radii of water-filled pore spaces in the soil become smaller. This process produces the general shape of the water-retention curve (also known as the ‘moisture characteristic’ or ‘water release’ curve), which relates Ψ_s to volumetric soil moisture content (θ). Critically, variation in soil physical properties can cause Ψ_s to differ by an order of magnitude across soil types, even if θ is the same^{10,11} (Fig. 2a).

Field observations of θ are common¹², but with a few exceptions^{9,13}, Ψ_s is rarely measured systematically in field research settings^{8,9}. The reasons why θ became the predominant metric for describing soil water status are not entirely clear⁸, but may reflect the fact that no single instrument captures the entire range of Ψ_s (from saturation to the very dry end), and sensors for measuring Ψ_s in the field have historically been associated with unique limitations and uncertainty^{8,14}.

Even if Ψ_s data were plentiful, strategies for relating θ to Ψ_s would still be necessary in models to connect water-balance equations with

¹O’Neill School of Public and Environmental Affairs, Indiana University Bloomington, Bloomington, IN, USA. ²Department of Geography, Indiana University Bloomington, Bloomington, IN, USA. ³Department of Environmental Science, Policy, and Management, University of California Berkeley, Berkeley, CA, USA.

⁴Department of Meteorology and Atmospheric Science and Earth and Environmental Systems Institute, The Pennsylvania State University, University Park, PA, USA. ⁵Life and Environmental Sciences Department, University of California Merced, Merced, CA, USA. ⁶Department of Earth System Science, Stanford University, Stanford, CA, USA. ⁷Laboratoire des Sciences du Climat et de l’Environnement, Paris, France. ⁸Southwest Watershed Research Center, USDA Agricultural Research Service, Tucson, AZ, USA. ⁹Department of Plant Science, The Pennsylvania State University, University Park, PA, USA.

¹⁰Environmental Sciences Division, Oak Ridge National Laboratory, Oak Ridge, TN, USA. ¹¹School of Natural Resources, University of Missouri, Columbia, MO, USA. ✉e-mail: knovick@indiana.edu

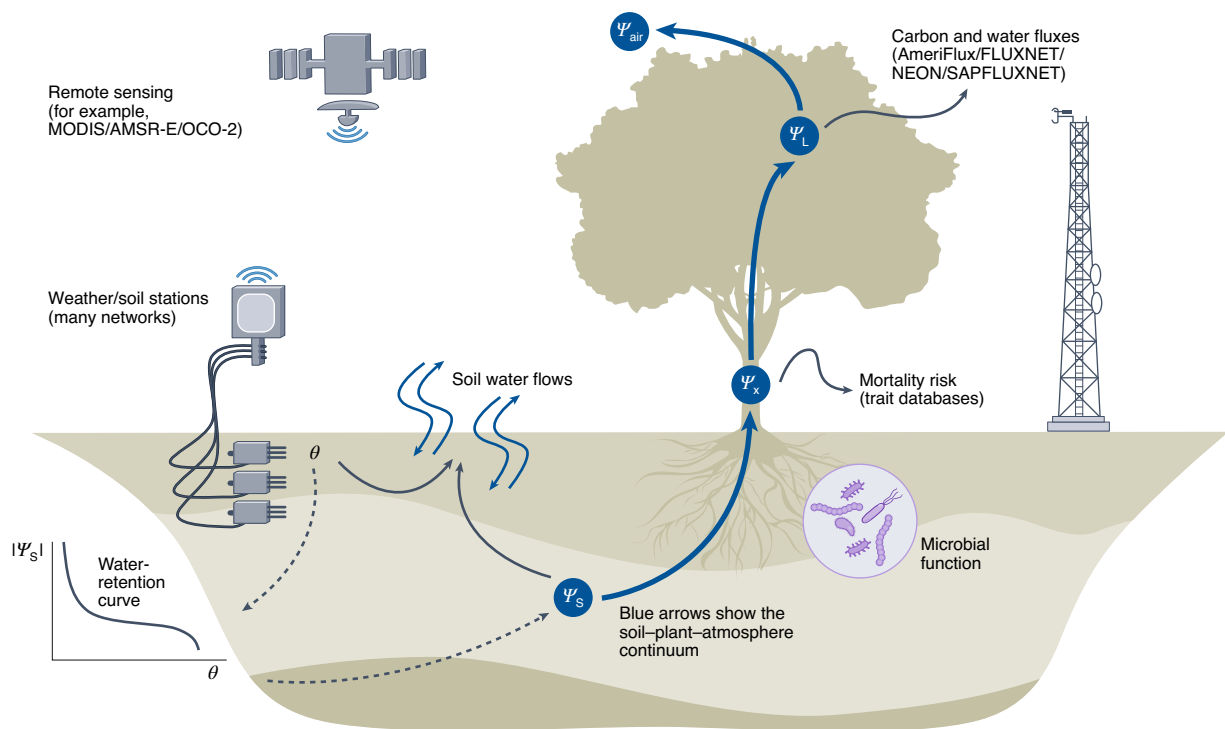


Fig. 1 | Ψ links environmental drivers to biophysical responses. Water flows downhill along gradients of Ψ in the soils (Ψ_s , where Ψ is relatively high, often >-1 MPa) through the stems (Ψ_x) to the leaves (Ψ_L , where potential is relatively low) and eventually to the air (Ψ_{air} , where it can be as low as -100 MPa). Ψ also directly controls key biological processes, including microbial function, mortality risk arising from damaged plant xylem, and plant-atmosphere gas exchange. While observations of environmental drivers, θ , and carbon and water fluxes are broadly accessible from environmental networks and remote sensing, Ψ time series are more discrete, sparse and generally not coordinated or discoverable.

potential-driven flows. Most hydrologic and land-surface models thus rely on water-retention-curve models¹⁵, with those proposed by refs.^{10,11} ranking high in popularity. Pedotransfer functions (PTFs) predict the parameters of water-retention-curve models using empirical equations driven by a limited set of soil characteristics (typically %sand, %clay and bulk density^{16–18}).

While developing PTFs is an active field¹⁵, PTF parameter distributions are poorly constrained and prevent confident transformation of θ to Ψ_s . For example, even relatively small variations in a single parameter of the van Genuchten model¹¹ cause Ψ_s to vary by an order of magnitude over a wide range of θ (Fig. 2b–d). Soil structure, which differs from soil texture and is governed by biophysical properties, may be a key omission in PTFs¹⁹ explaining some of this uncertainty. For example, growth of roots and mycorrhizae into soil pores, and deposition of root exudates, increase overall water retention^{20,21}, and macropores can create preferred flow pathways that are challenging to incorporate into PTFs. Moreover, depth into the soil may also affect hydraulic properties by controlling connectivity with root systems and through slowly evolving changes in soil morphology. Finally, most PTFs assume that the water-retention curve is static, but many relevant processes occurring in natural landscapes (including drying–rewetting cycles, fire, and management shifts) may cause time-dependent hysteresis of the water-retention curve^{22–24}.

This uncertainty linked to PTFs propagates through water-cycle models in highly consequential ways.^{25,26} Previous work performed in the Shale Hills Critical Zone Observatory confirms that van Genuchten model¹¹ parameters are the dominant source of model uncertainty in a coupled three-dimensional (3D) land-surface and hydrological model²⁷, and that water-retention-curve parameters must be measured locally and optimized through data assimilation²⁸ for watershed hydrologic variables to be predicted with any degree

of certainty²⁹. Here, using a popular 1D water-balance model, we further demonstrate that uncertainty in a single PTF parameter drives large uncertainty in modelled predictions of evapotranspiration, soil moisture and Ψ_s (Fig. 2e).

The parameters of the water-retention curve are also key sources of uncertainty explaining variability in carbon cycle fluxes from global-scale land-surface models. In this study, we used a global sensitivity experiment³⁰ to explore the variability of these parameters along with other key parameters of the ORCHIDEE land-surface model^{31,32} (see Methods for details). The parameters of the water-retention curve explained between 10% and 32% of the modelled GPP variance across three diverse sites (Fig. 3). Moreover, when considering the wider set of soil hydrology parameters (including the hydraulic conductivity, field capacity and permanent wilting point of the soil), the percentage of explained GPP variance increased to 22–53% across sites.

The dearth of information about Ψ_s is not only a problem for models, but also confounds observation-driven work. Because θ is widely measured, and Ψ_s is not, it is extremely common to see key response variables such as carbon and water fluxes explained as a function of measured θ ^{33–35}. These relationships are usually nonlinear and threshold driven^{36,37}. This is not surprising, as these responses embed site-to-site variability in the water-retention curve, which itself is nonlinear and threshold driven (Fig. 2a–d). The shape of these response functions thus depends very much on whether Ψ_s or θ is chosen as the driving variable³⁸. Indeed, the relationship between gross primary productivity (GPP) and soil water status is more linear and less spatially heterogeneous when Ψ_s , as opposed to θ , appears on the x axis (Fig. 4). Likewise, substantial skill in predicting soil respiration can be gained when model functions are driven explicitly by Ψ_s (ref.³). Thus, more abundant and aggregated site-level Ψ_s information could reduce conceptual

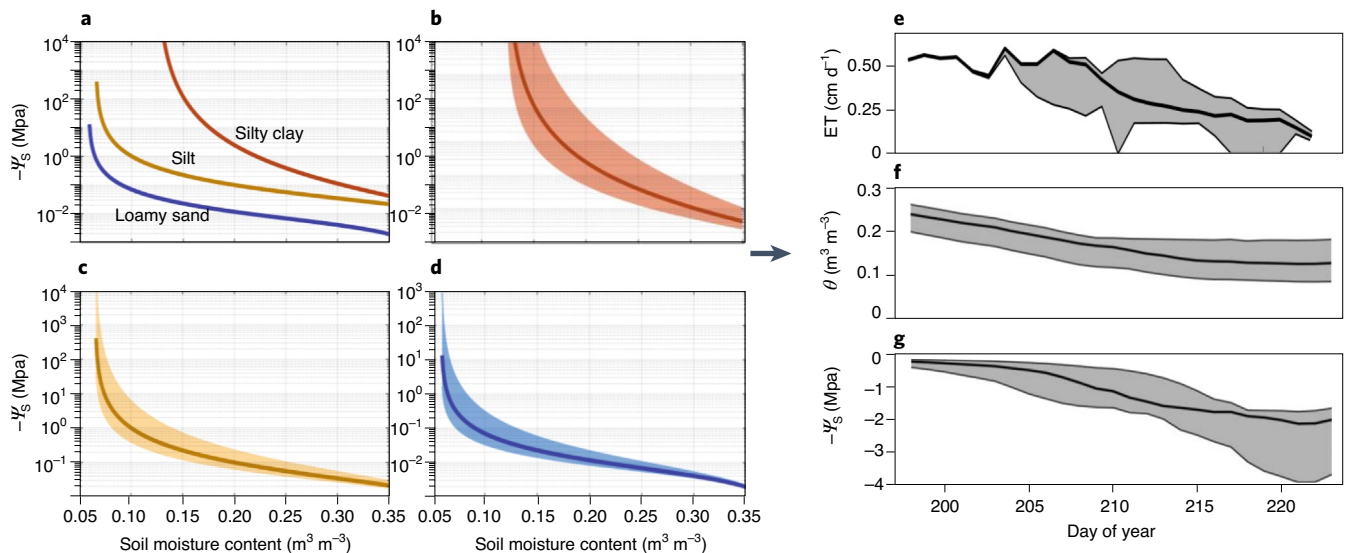


Fig. 2 | Water-retention curve and PTF uncertainty. **a**, Across three soil types, Ψ_s can differ by an order of magnitude for a given θ (with curves generated from the van Genuchten model¹¹; see Methods). **b–d**, The uncertainty in the water-retention curve attributable to PTF parameter uncertainty. The shaded area shows the 90% confidence interval due solely to variation in a single parameter of the van Genuchten model (the n shape parameter, which is linked to pore size) within just one standard deviation of its reported distribution for each soil class from a popular PTF¹⁸: silty clay (**b**), silt (**c**) and loamy sand (**d**). Thick lines in **b–d** are the same as in **a**. The PTF-driven uncertainty in the water-retention curve propagates into large uncertainty for modelled fluxes and pools. **e–g**, Specifically, variation in the van Genuchten n parameter within again just one standard deviation of its reported range¹⁸ causes the 90% confidence intervals on modelled evapotranspiration (ET) (**e**), θ (**f**) and Ψ_s (**g**) (shaded grey areas) to vary by a magnitude comparable to the mean value of each parameter (thick black line). Simulations were run using the HYDRUS 1D⁷⁹ model for a forest site in Indiana, USA⁸⁰, during a drought event (see Methods for details).

uncertainty about how ecosystem fluxes respond to soil water deficits and permit other sources of spatio-temporal variability to be more discernable.

Plant Ψ : key concepts and controversies

The effective radii of evaporating water surfaces within plant cell walls are extremely small, resulting in tension forces strong enough to pull water upwards from soils, where it is already tightly bound, to the leaves. Thus, the difference between Ψ_L and Ψ_s is the driving force for transpiration, which is closely coupled with photosynthetic carbon uptake. Moreover, Ψ_x , which is coupled with Ψ_L , interacts with anatomical features of the plant's water transport system to determine the risk of xylem embolism that can lead to mortality^{6,7,39–41}. Stomatal regulation of gas exchange is also critical for buffering plants from the very low Ψ of the atmosphere (see Fig. 1), which is extremely sensitive to relative humidity⁴².

Historically, observations of plant Ψ have been limited to manually collected 'snapshots' (for example, with a pressure chamber⁴³). These data have proved indispensable for shaping our theoretical understanding of how plants respond to soil water stress^{6,7,40,44}. However, because pressure-chamber measurements are destructive and labour intensive, they are typically limited to weekly or seasonal temporal resolutions. While the weekly timescale is well matched to soil drying, it is too coarse to capture faster-acting hydrodynamic processes, including stomatal response to vapour pressure deficit (VPD⁴⁵) and the depletion and refilling of plant water pools over the course of a day⁴⁶. Moreover, with some exceptions⁴⁷, Ψ_L and Ψ_x are not often monitored over long periods (for example, years to decades), and centralized databases and networks for time series of Ψ do not yet exist.

The discrete and undiscoverable nature of plant Ψ observations limits our ability to characterize the distributions of the minimum plant Ψ that are so critical for determining plant mortality risk⁴¹. The gap also limits understanding of how plant Ψ and Ψ_s are

coordinated and coupled. For example, a fundamental assumption in plant eco-physiology is that Ψ_L and Ψ_x are equilibrated with Ψ_s across the root zone in pre-dawn hours⁴⁸. This assumption has allowed eco-physiologists to circumvent the Ψ_s data scarcity problem by relying on pre-dawn Ψ_L observations as a proxy for root-zone Ψ_s —an approach that treats the plants as an instrument for recording the soil water environment. Yet experiments have shown that night-time transpiration—while small—can still occur^{49,50}, lowering pre-dawn Ψ_L and decoupling it from Ψ_s (ref. ⁵¹). Synthetic assessments of pre-dawn equilibrium are hindered by the absence of nocturnal Ψ_L observations collected together with data on Ψ_s and/or stem water flows (for example, from sap flux), or collected frequently enough to determine whether stationarity in pre-dawn Ψ_L , which should be a hallmark of equilibrium, has been achieved.

Likewise, the Ψ information gap limits understanding of how Ψ_s and plant Ψ are coupled at mid-day. The relationship between mid-day Ψ_L and the root-zone Ψ_s is frequently used to classify plant water-use strategies^{44,52,53}. For example, plants with conservative water-use strategies ('isohydric' species) close stomata quickly as Ψ_s declines, whereas 'anisohydric' plants keep stomata open longer, sustaining gas exchange but with more rapid declines in Ψ_L that may increase the risk of xylem embolism. The (an)isohydry framework is popular but controversial, with several studies highlighting critical interactions with other environmental drivers beyond Ψ_s (refs. ^{54–56}), including VPD⁵⁷. Moreover, coordinated observations of sap flow, enhanced with data on Ψ_s and Ψ_x , hold great promise for understanding how the dynamics of hydraulic conductance of different plant organs influence whole-plant hydraulic physiology⁵⁸. Plant hydraulics schemes relying on concepts such as isohydry are rapidly being incorporated in hydrologic and Earth system models^{59–61}. Benchmarking and testing these schemes would benefit from open and spatially representative databases of plant Ψ and Ψ_s time series, measured together at a temporal frequency (for example, hourly) over which key drivers such as VPD vary.

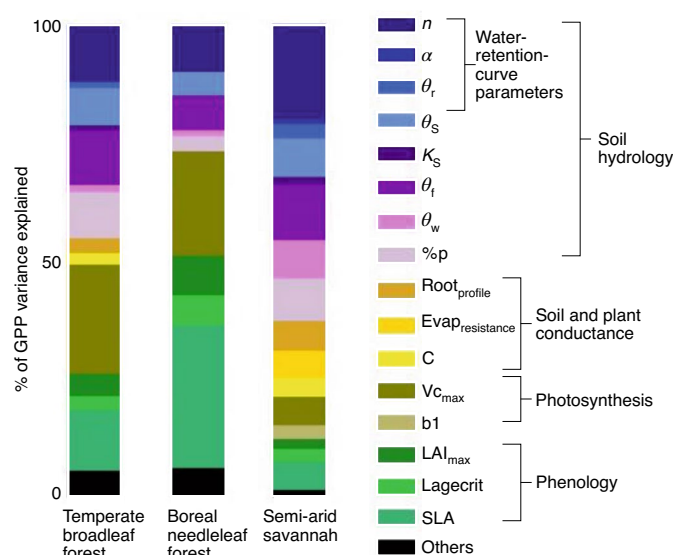


Fig. 3 | Water-retention-curve parameters are a key source of land-surface model uncertainty. A sensitivity analysis of key model parameters of the ORCHIDEE land-surface model^{31,32} was performed to demonstrate the relative importance of each parameter in simulating daily GPP at three contrasting FLUXNET sites. **a**, A temperate broadleaf forest (Harvard Forest, FLUXNET code US-Ha1⁸¹). **b**, A boreal needleleaf forest (Sodankylä, FI-Sod⁸²). **c**, A semi-arid savannah (Demokeya, SD-Dem⁸³). The Sobol method³⁰ was used to perform the sensitivity analysis; this method is based on variance decomposition and is able to capture interactions between parameters. More details can be found in Methods.

Coordinated observation of plant Ψ and Ψ_s could also offer new perspectives on the critical role of root hydraulic function. Pre-dawn observations of Ψ_L and Ψ_x from multiple depths could reveal interspecific patterns in functional rooting depth—a trait that is difficult to measure by other means and partially responsible for model difficulty in capturing plant drought responses⁶². When complemented with data on Ψ_x and/or root sap flow, profile observations of Ψ_s would also illuminate the important but poorly understood consequences of hydraulic redistribution of water from wetter to drier soil layers through plant roots^{53,64}. While root Ψ_x is difficult to measure with pressure chambers, it could be monitored more easily with psychrometers or other techniques for continuous observation of plant Ψ_x . Data on root Ψ_x , especially when paired with laboratory-derived root xylem vulnerability curves, would also be useful for understanding the dynamics of root hydraulic conductance, noting that roots may be among the most vulnerable components of the plant hydraulic system^{65,66}. Finally, differences in Ψ_s and root Ψ_x could also improve our understanding of gradients in Ψ occurring at the root–soil interface⁶⁷.

Strategies to address the Ψ information gap

Recent advances in measurement technology have substantially improved the ease and reliability of Ψ_s observations. In the lab, sensor improvement has reduced the time necessary to generate the ‘wet end’ of the water-retention curve⁶⁸. A second instrument, typically a dew-point potentiometer, is required to capture the dry end of the curve, but this step proceeds relatively quickly. While the instrumentation and expertise necessary to characterize water-retention curves may be siloed within soil science disciplines, this barrier could be easily overcome through cooperative arrangements and/or knowledge transfer. At the same time, technology is improving for more confident observation of Ψ_s in situ⁸. Tensiometers, which are accurate when soil is relatively wet (for example, $\Psi_s > -0.1$ MPa),

are widely used in agricultural settings for the purposes of irrigation scheduling. In the drier range, soil matric potential can be measured using psychrometry or from dielectric measurements, with several commercial sensors available at a relatively low cost (for example, the Teros 21 product, Meter Group). While the accuracy of sensors such as these is greatest when Ψ_s is above -2 MPa, this is still lower than the wilting point of many plant species⁸.

With respect to plants, psychrometers permitting continuous and long-term observation of both Ψ_L and Ψ_x are becoming more widely and commercially available (for example, the PSY1 products, ICT International), drawing from a long history of psychrometric approaches for measuring plant Ψ (ref. ⁶⁹). Stem psychrometers can now be deployed on branches and boles of some species for weeks to months at a time⁵⁵, and evidence is mounting that high-frequency Ψ_L and Ψ_x data can indeed improve our understanding of plant water-use strategies and dynamics^{55,70}. Psychrometers are still relatively expensive, best suited for broadleaf and non-resinous species and sensitive to biases linked to temperature fluctuations and wounding effects. Thus, for now, psychrometer data are best viewed as complementary to pressure-chamber measurements. Nonetheless, for many plants, these instruments allow for the collection of Ψ_L and/or Ψ_x data at the hourly timescales necessary to be harmonized with observed carbon and water fluxes (for example, from sap flux and flux towers) and to more rigorously test model frameworks.

Ultimately, addressing environmental questions at policy- and management-relevant scales requires the collection and standardization of observations across many sites. This need has motivated the recent development of many environmental observation networks, including highly centralized initiatives such as the National Science Foundation’s National Ecological Observatory Network⁷¹, as well as more bottom-up networks such as AmeriFlux⁷² and FLUXNET⁷³ and the new international SAPFLUXNET network⁷⁴. Other approaches include ‘network-of-networks’ cyberinfrastructure such as the International Soil Moisture Network,¹³ which aggregates soil moisture observations from dozens of individual networks.

Both bottom-up and top-down approaches could be useful for building new Ψ networks. On the one hand, centralized and standardized deployment of new Ψ sensors, ideally in locations that are already nodes of other networks, would have the advantage of uniformity in instrumentation and data quality control that facilitates cross-site synthesis. On the other hand, a community-driven effort to aggregate and redistribute both existing and new Ψ data could follow the highly successful ‘coalition’ model employed by networks such as AmeriFlux⁷², increasing the discoverability of data while allowing room for innovation at the site level. Even a concerted effort to generate and/or collect laboratory-based water-retention curves from existing network sites could substantially constrain how much of the nonlinearity in the response of fluxes to observed soil water content can be explained by soil physics (for example, see Fig. 4). The success of a Ψ network would be maximized with (1) a focus on collecting data from sites that also support continuous plant- and/or stand-scale carbon and water fluxes, (2) cyberinfrastructure to support the discoverability and distribution of these databases, (3) a focus in at least some locations on within-site spatial heterogeneity in Ψ dynamics to better understand how many observation points (and at what depths) are necessary to substantially improve model skill, and (4) training programmes, such as summer short courses or distributed graduate seminars, to transfer knowledge about how to interpret network observations and to share best practices for sensor deployment.

Even with well-developed observation networks, it is not possible to measure key physiological variables such as Ψ everywhere and all the time. Thus, strategies for linking these variables to proxies observable from space are required for regional- and

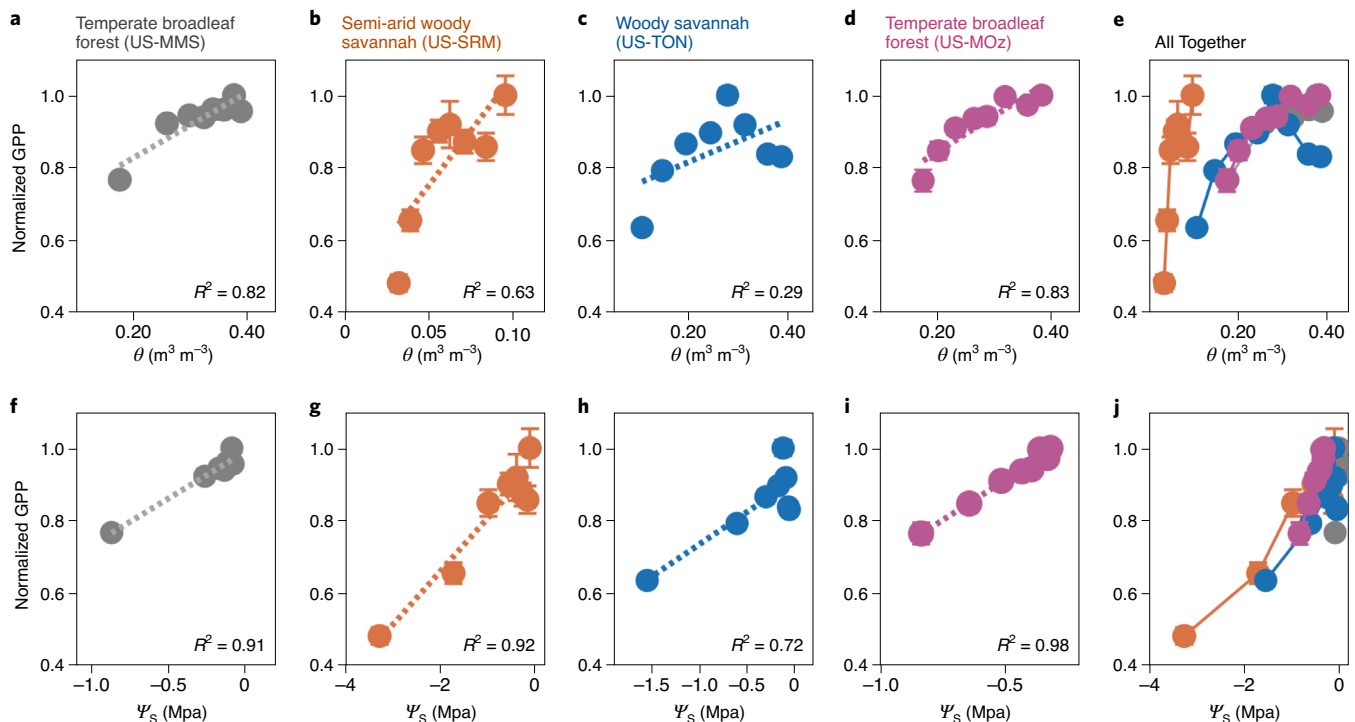


Fig. 4 | Ψ_s better explains variability in GPP when compared with θ . **a–j**, The relationship between GPP (normalized by its well-watered rate) and Ψ_s (**f–j**) is more linear than the relationship between GPP and θ (**a–e**) across four AmeriFlux sites for which site-specific water-retention curves were measured^{38,84–86}: a temperate broadleaf forest (US-MMS) (**a,f**), a semi-arid woody savannah (US-SRM) (**b,g**), a woody savannah (US-TON) (**c,h**), another temperate broadleaf forest (US-MOZ) (**d,i**), and all together (**e,j**). Moreover, cross-site heterogeneity in the response functions is reduced when it is Ψ_s , as opposed to θ , on the x axis (compare **e** with **j**). GPP estimates were obtained from AmeriFlux, with site codes given in parentheses. Error bars indicate one standard error of the mean, which is quite small for some of the binned averages. See Methods for more details.

continental-scale work, with microwave remote sensing representing a particularly promising approach. Microwave observations can be used to determine vegetation optical depth (VOD), which is sensitive to plant water content⁷⁵ and should be monotonically related to Ψ_L ^{76,77}. Comparison of observed Ψ_L with either space-borne⁷⁸ or tower-based⁷⁰ radiometry confirms that VOD and Ψ_L follow similar dynamics, especially after accounting for the effect of changing biomass and leaf area. However, the exact relationship between VOD and Ψ_L is influenced by vegetation type⁷⁶, and further study of this relationship is currently hindered by the sparsity of Ψ_L data.

Importantly, microwave remote-sensing observations can be made at night, which raises the question of whether nocturnal microwave remote sensing of Ψ_L can be used to infer dynamics of root-zone Ψ_s . Answering this question requires a critical understanding of when and where pre-dawn Ψ_L is equilibrated with root-zone Ψ_s . This knowledge gap can be addressed with network observations of Ψ_L from psychrometry or observations of plant Ψ and Ψ_s collected in the same site, which could then guide the design and interpretation of both tower- and satellite-mounted microwave remote-sensing systems. The approach will also require further refinement of retrieval algorithms for separating the contribution of plant and soil water content, for example, by leveraging emerging approaches for the remote sensing of vegetation structure⁷⁷.

In conclusion, we have highlighted how more numerous, discoverable and continuous observations of Ψ_s and plant Ψ can not only improve our conceptual understanding of biophysical processes throughout the soil–plant–atmosphere continuum, but also serve as a much-needed new tool for benchmarking and calibrating hydrologic and land-surface models and remote-sensing products. While in situ and site-specific observations of Ψ_s , Ψ_L and Ψ_x may not yet be easy, recent advancements in sensor technology have certainly

made them easier than in decades past. The time is right for a new focus on the collection of these data in the field and the development of new networks to aggregate observations across sites complemented by new approaches for integrating these observations into Earth system models.

Online content

Any methods, additional references, Nature Research reporting summaries, source data, statements of data availability and associated accession codes are available at [<https://doi.org/10.1038/s41561-022-00909-2>].

Received: 1 April 2021; Accepted: 2 February 2022;

Published online: 11 March 2022

Reference

- Brutsaert, W. *Hydrology: An Introduction* (Cambridge Univ. Press, 2005).
- Philip, J. Plant water relations: some physical aspects. *Annu. Rev. Plant Physiol.* **17**, 245–268 (1966).
- Ghezzehei, T. A., Sulman, B., Arnold, C. L., Bogie, N. A. & Berhe, A. A. On the role of soil water retention characteristic on aerobic microbial respiration. *Biogeosciences* **16**, 1187–1209 (2019).
- Boyer, J. Differing sensitivity of photosynthesis to low leaf water potentials in corn and soybean. *Plant Physiol.* **46**, 236–239 (1970).
- Jarvis, P. The interpretation of the variations in leaf water potential and stomatal conductance found in canopies in the field. *Phil. Trans. R. Soc. Lond. B* **273**, 593–610 (1976).
- Choat, B. et al. Global convergence in the vulnerability of forests to drought. *Nature* **491**, 752–755 (2012).
- Tyree, M. T. & Sperry, J. S. Vulnerability of xylem to cavitation and embolism. *Annu. Rev. Plant Biol.* **40**, 19–36 (1989).
- Whalley, W., Ober, E. & Jenkins, M. J. J. Measurement of the matric potential of soil water in the rhizosphere. *J. Exp. Biol.* **64**, 3951–3963 (2013).

9. Yu, H., Yang, P. & Lin, H. Spatiotemporal patterns of soil matric potential in the Shale Hills Critical Zone Observatory. *Vadose Zone J.* <https://doi.org/10.2136/vzj2014.11.0167> (2015).
10. Campbell, G. S. A simple method for determining unsaturated conductivity from moisture retention data. *Soil Sci.* **117**, 311–314 (1974).
11. van Genuchten, M. T. A closed-form equation for predicting the hydraulic conductivity of unsaturated soils. *Soil Sci. Soc. Am. J.* **44**, 892–898 (1980).
12. Dorigo, W. et al. The International Soil Moisture Network: a data hosting facility for global in situ soil moisture measurements. *Hydrol. Earth Syst. Sci.* **15**, 1675–1698 (2011).
13. Scott, B. L. et al. New soil property database improves Oklahoma Mesonet soil moisture estimates. *J. Atmos. Ocean. Technol.* **30**, 2585–2595 (2013).
14. Campbell, G. S. Soil water potential measurement: an overview. *Irrig. Sci.* **9**, 265–273 (1988).
15. Van Looy, K. et al. Pedotransfer functions in Earth system science: challenges and perspectives. *Rev. Geophys.* **55**, 1199–1256 (2017).
16. Clapp, R. B. & Hornberger, G. M. Empirical equations for some soil hydraulic properties. *Water Resour. Res.* **14**, 601–604 (1978).
17. Cosby, B., Hornberger, G., Clapp, R. & Ginn, T. A statistical exploration of the relationships of soil moisture characteristics to the physical properties of soils. *Water Resour. Res.* **20**, 682–690 (1984).
18. Zhang, Y. & Schaap, M. G. Weighted recalibration of the Rosetta pedotransfer model with improved estimates of hydraulic parameter distributions and summary statistics (Rosetta3). *J. Hydrol.* **547**, 39–53 (2017).
19. Faticchi, S. et al. Soil structure is an important omission in Earth system models. *Nat. Commun.* **11**, 522 (2020).
20. Ghezzehei, T. A. & Albaladejo, A. A. Spatial distribution of rhizodeposits provides built-in water potential gradient in the rhizosphere. *Ecol. Modell.* **298**, 53–63 (2015).
21. Leung, A. K., Garg, A. & Ng, C. W. W. Effects of plant roots on soil-water retention and induced suction in vegetated soil. *Eng. Geol.* **193**, 183–197 (2015).
22. Caplan, J. S. et al. Decadal-scale shifts in soil hydraulic properties as induced by altered precipitation. *Sci. Adv.* **5**, eaau6635 (2019).
23. Peña-Sancho, C., López, M., Gracia, R. & Moret-Fernández, D. Effects of tillage on the soil water retention curve during a fallow period of a semiarid dryland. *Soil Res.* **55**, 114–123 (2017).
24. Stoof, C. R., Wesseling, J. G. & Ritsema, C. J. Effects of fire and ash on soil water retention. *Geoderma* **159**, 276–285 (2010).
25. Gutmann, E. & Small, E. The effect of soil hydraulic properties vs. soil texture in land surface models. *Geophys. Res. Lett.* **32**, L02402 (2005).
26. Weihermüller, L. et al. Choice of pedotransfer functions matters when simulating soil water balance fluxes. *J. Adv. Model. Earth Syst.* **13**, e2020MS002404 (2021).
27. Shi, Y., Davis, K. J., Zhang, F. & Duffy, C. J. Evaluation of the parameter sensitivities of a coupled land surface hydrologic model at a critical zone observatory. *J. Hydrometeorol.* **15**, 279–299 (2014).
28. Shi, Y., Davis, K. J., Zhang, F., Duffy, C. J. & Yu, X. J. Parameter estimation of a physically-based land surface hydrologic model using an ensemble Kalman filter: a multivariate real-data experiment. *Adv. Water Res.* **83**, 421–427 (2015).
29. Shi, Y. et al. Simulating high-resolution soil moisture patterns in the Shale Hills watershed using a land surface hydrologic model. *Hydrol. Process.* **29**, 4624–4637 (2015).
30. Sobol, I. M. Global sensitivity indices for nonlinear mathematical models and their Monte Carlo estimates. *Math. Comput. Simul.* **55**, 271–280 (2001).
31. Boucher, O. et al. Presentation and evaluation of the IPSL-CM6A-LR climate model. *J. Adv. Model. Earth Syst.* **12**, e2019MS002010 (2020).
32. Lurton, T. et al. Implementation of the CMIP6 forcing data in the IPSL-CM6A-LR model. *J. Adv. Model. Earth Syst.* **12**, e2019MS001940 (2020).
33. Green, J. K. et al. Large influence of soil moisture on long-term terrestrial carbon uptake. *Nature* **565**, 476–479 (2019).
34. Jung, M. et al. Recent decline in the global land evapotranspiration trend due to limited moisture supply. *Nature* **467**, 951–954 (2010).
35. Novick, K. A. et al. The increasing importance of atmospheric demand for ecosystem water and carbon fluxes. *Nat. Clim. Change* **6**, 1023–1027 (2016).
36. Feldman, A. F., Short Gianotti, D. J., Trigo, I. F., Salvucci, G. D. & Entekhabi, D. Satellite-based assessment of land surface energy partitioning–soil moisture relationships and effects of confounding variables. *Water Resour. Res.* **55**, 10657–10677 (2019).
37. Stocker, B. D. et al. Quantifying soil moisture impacts on light use efficiency across biomes. *N. Phytol.* **218**, 1430–1449 (2018).
38. Baldocchi, D. D., Xu, L. & Kiang, N. How plant functional-type, weather, seasonal drought, and soil physical properties alter water and energy fluxes of an oak–grass savanna and an annual grassland. *Agric. For. Meteorol.* **123**, 13–39 (2004).
39. Trugman, A. T., Anderegg, L. D., Shaw, J. D. & Anderegg, W. R. Trait velocities reveal that mortality has driven widespread coordinated shifts in forest hydraulic trait composition. *Proc. Natl Acad. Sci. USA* **117**, 8532–8538 (2020).
40. McDowell, N. et al. Mechanisms of plant survival and mortality during drought: why do some plants survive while others succumb to drought? *N. Phytol.* **178**, 719–739 (2008).
41. Martínez-Vilalta, J. et al. Towards a statistically robust determination of minimum water potential and hydraulic risk in plants. *New Phytol.* **232**, 404–417 (2021).
42. Taiz, L., Zeiger, E., Møller, I. M. & Murphy, A. *Plant Physiology and Development* 6th edn (Sinauer Associates, 2015).
43. Scholander, P. F., Bradstreet, E. D., Hemmingen, E. & Hammel, H. Sap pressure in vascular plants: negative hydrostatic pressure can be measured in plants. *Science* **148**, 339–346 (1965).
44. Martínez-Vilalta, J., Poyatos, R., Aguadé, D., Retana, J. & Mencuccini, M. A new look at water transport regulation in plants. *N. Phytol.* **204**, 105–115 (2014).
45. Grossiord, C. et al. Plant responses to rising vapor pressure deficit. *N. Phytol.* **226**, 1550–1566 (2020).
46. Matheny, A. M. et al. Observations of stem water storage in trees of opposing hydraulic strategies. *Ecosphere* <https://doi.org/10.1890/es15-00170.1> (2015).
47. Wood, J. D., Knapp, B. O., Muzika, R.-M., Stambaugh, M. C. & Gu, L. The importance of drought–pathogen interactions in driving oak mortality events in the Ozark Border Region. *Environ. Res. Lett.* **13**, 015004 (2018).
48. Hinckley, T. M., Lassoie, J. P. & Running, S. W. Temporal and spatial variations in the water status of forest trees. *For. Sci.* **24**, a0001–z0001 (1978).
49. Marks, C. O. & Lechowicz, M. J. The ecological and functional correlates of nocturnal transpiration. *Tree Physiol.* **27**, 577–584 (2007).
50. O’Keefe, K. & Nippert, J. B. Drivers of nocturnal water flux in a tallgrass prairie. *Funct. Ecol.* **32**, 1155–1167 (2018).
51. Donovan, L., Linton, M. & Richards, J. Predawn plant water potential does not necessarily equilibrate with soil water potential under well-watered conditions. *Oecologia* **129**, 328–335 (2001).
52. Kannenberg, S. A. et al. Opportunities, challenges and pitfalls in characterizing plant water-use strategies. *Funct. Ecol.* **36**, 24–37 (2022).
53. Oliveira, R. S. et al. Linking plant hydraulics and the fast–slow continuum to understand resilience to drought in tropical ecosystems. *New Phytol.* **230**, 904–923 (2021).
54. Feng, X. et al. Beyond isohydricity: the role of environmental variability in determining plant drought responses. *Plant Cell Environ.* **42**, 1104–1111 (2019).
55. Guo, J. S., Hultine, K. R., Koch, G. W., Kropp, H. & Ogle, K. Temporal shifts in iso/anisohydry revealed from daily observations of plant water potential in a dominant desert shrub. *N. Phytol.* **225**, 713–726 (2020).
56. Hochberg, U., Rockwell, F. E., Holbrook, N. M. & Cochard, H. Iso/anisohydry: a plant–environment interaction rather than a simple hydraulic trait. *Trends Plant Sci.* **23**, 112–120 (2018).
57. Novick, K. A., Konings, A. G. & Gentile, P. Beyond soil water potential: an expanded view on isohydricity including land–atmosphere interactions and phenology. *Plant Cell Environ.* **42**, 1802–1815 (2019).
58. McCulloh, K. A. et al. A dynamic yet vulnerable pipeline: integration and coordination of hydraulic traits across whole plants. *Plant Cell Environ.* **42**, 2789–2807 (2019).
59. Kennedy, D. et al. Implementing plant hydraulics in the Community Land Model, version 5. *J. Adv. Model. Earth Syst.* **11**, 485–513 (2019).
60. Mirfenderesgi, G., Matheny, A. M. & Bohrer, G. Hydrodynamic trait coordination and cost–benefit trade-offs throughout the isohydric–anisohydric continuum in trees. *Ecohydrology* **12**, e2041 (2019).
61. Xu, X., Medvigy, D., Powers, J. S., Becknell, J. M. & Guan, K. Diversity in plant hydraulic traits explains seasonal and inter-annual variations of vegetation dynamics in seasonally dry tropical forests. *N. Phytol.* **212**, 80–95 (2016).
62. De Kauwe, M. G. et al. Do land surface models need to include differential plant species responses to drought? Examining model predictions across a mesic–xeric gradient in Europe. *Biogeosciences* **12**, 7503–7518 (2015).
63. Meinzer, F. C. et al. Converging patterns of uptake and hydraulic redistribution of soil water in contrasting woody vegetation types. *Tree Physiol.* **24**, 919–928 (2004).
64. Scott, R. L., Cable, W. L. & Hultine, K. R. The ecohydrologic significance of hydraulic redistribution in a semiarid savanna. *Water Resour. Res.* **44**, W02440 (2008).
65. Tyree, M. T. & Ewers, F. W. The hydraulic architecture of trees and other woody plants. *N. Phytol.* **119**, 345–360 (1991).
66. Johnson, D. M. et al. A test of the hydraulic vulnerability segmentation hypothesis in angiosperm and conifer tree species. *Tree Physiol.* **36**, 983–993 (2016).
67. Lehto, T. & Zwiazek, J. J. Ectomycorrhizas and water relations of trees: a review. *Mycorrhiza* **21**, 71–90 (2011).
68. Bezerra-Coelho, C. R., Zhuang, L., Barbosa, M. C., Soto, M. A. & Van Genuchten, M. T. Further tests of the HYPROP evaporation method for estimating the unsaturated soil hydraulic properties. *J. Hydrol. Hydromech.* **66**, 161–169 (2018).

69. Wullschlegel, S., Dixon, M. & Oosterhuis, D. Field measurement of leaf water potential with a temperature-corrected in situ thermocouple psychrometer. *Plant Cell Environ.* **11**, 199–203 (1988).
70. Holtzman, N. M. et al. L-band vegetation optical depth as an indicator of plant water potential in a temperate deciduous forest stand. *Biogeosciences* **18**, 739–753 (2021).
71. Nagy, R. C. et al. Harnessing the NEON data revolution to advance open environmental science with a diverse and data-capable community. *Ecosphere* **12**, e03833 (2021).
72. Novick, K. A. et al. The AmeriFlux network: a coalition of the willing. *Agric. For. Meteorol.* **249**, 444–456 (2018).
73. Baldocchi, D. 'Breathing' of the terrestrial biosphere: lessons learned from a global network of carbon dioxide flux measurement systems. *Aust. J. Bot.* **56**, 1–26 (2008).
74. Poyatos, R. et al. Global transpiration data from sap flow measurements: the SAPFLUXNET database. *Earth Syst. Sci. Data* **13**, 2607–2649 (2021).
75. Jackson, T. & Schmugge, T. Vegetation effects on the microwave emission of soils. *Remote Sens. Environ.* **36**, 203–212 (1991).
76. Konings, A. G., Rao, K. & Steele-Dunne, S. C. Macro to micro: microwave remote sensing of plant water content for physiology and ecology. *N. Phytol.* **223**, 1166–1172 (2019).
77. Konings, A. G. et al. Detecting forest response to droughts with global observations of vegetation water content. *Glob. Change Biol.* <https://doi.org/10.1111/gcb.15872> (2021).
78. Momen, M. et al. Interacting effects of leaf water potential and biomass on vegetation optical depth. *J. Geophys. Res. Biogeosci.* **122**, 3031–3046 (2017).
79. Simunek, J., Van Genuchten, M. T. & Sejna, M. *The HYDRUS-1D Software Package for Simulating the One-Dimensional Movement of Water, Heat, and Multiple Solutes in Variably-Saturated Media* (Dept Environ. Sci. Univ. California Riverside, 2005).
80. Naylor, S., Letsinger, S., Ficklin, D., Ellett, K. & Olyphant, G. A hydrogeological approach to quantifying groundwater recharge in various glacial settings of the mid-continental USA. *Hydrol. Process.* **30**, 1594–1608 (2016).
81. Urbanski, S. et al. Factors controlling CO₂ exchange on timescales from hourly to decadal at Harvard Forest. *J. Geophys. Res. Biogeosci.* **112**, G02020 (2007).
82. Thum, T. et al. Parametrization of two photosynthesis models at the canopy scale in a northern boreal Scots pine forest. *Tellus B* **59**, 874–890 (2007).
83. Ardö, J., Mölder, M., El-Tahir, B. A. & Elkhidir, H. A. M. Seasonal variation of carbon fluxes in a sparse savanna in semi arid Sudan. *Carbon Balance Manage.* **3**, 7 (2008).
84. Roman, D. T. et al. The role of isohydric and anisohydric species in determining ecosystem-scale response to severe drought. *Oecologia* **179**, 641–654 (2015).
85. Fu, C. et al. Combined measurement and modeling of the hydrological impact of hydraulic redistribution using CLM4.5 at eight AmeriFlux sites. *Hydrol. Earth Syst. Sci.* **20**, 2001–2018 (2016).
86. Liang, J. et al. Evaluating the E3SM land model version 0 (ELMv0) at a temperate forest site using flux and soil water measurements. *Geosci. Model Dev.* **12**, 1601–1612 (2019).

Publisher's note Springer Nature remains neutral with regard to jurisdictional claims in published maps and institutional affiliations.

© Springer Nature Limited 2022

Methods

Water-retention-curve uncertainty. The water-retention curves in Fig. 2 were created using the van Genuchten water-retention curve model¹¹ relating Ψ_s to θ . As described in more detail in the Supplementary Information, most parameters of the model were held constant within each soil type, specified as the mean values reported in the updated ROSETTA PTF¹⁸ (Supplementary Table 1). The ‘ n ’ parameter—a key shape parameter of the van Genuchten model—was allowed to vary by randomly selecting a value from a uniform distribution bounded by ± 1 standard deviation as reported for the ROSETTA PTF¹⁸. Overall, this was a conservative approach; drawing the values of n from the full distribution reported for each soil type expands the range of predicted Ψ_s by orders of magnitude.

The HYDRUS 1D simulations. Uncertainty in the water-retention curve linked to pedotransfer uncertainty (for example, as Fig. 2a–d) was propagated through predictions of Ψ_s and θ (at depths of 15 cm) and surface evapotranspiration (cm d^{-1}) using the HYDRUS 1D soil water-dynamics model⁷⁹. Fifty simulations were performed for the Bradford Woods deciduous forest site in south-central Indiana, where the HYDRUS 1D model had been previously calibrated⁸⁰. In general, model settings were left unchanged, with a few exceptions as discussed in more detail in the Supplementary Information. The soil at Bradford Woods is characterized by a 40-cm-depth AP (plowed A) horizon dominated by sandy loam and a BW (weathered B) horizon dominated by silt loam from a depth of 40 cm to 208 cm. The very bottom of the soil layer (depths 208–230 cm) was prescribed to be clay loam. The parameters of the van Genuchten model used in the HYDRUS simulations are shown in Supplementary Table 2, where again most were held constant, but n varied for the sandy and silt loam layers by drawing it from within one standard deviation of its distribution reported in the updated ROSETTA PTF¹⁸. The shaded areas in Fig. 2e,f thus illustrate the resulting variations in evapotranspiration, Ψ_s and θ due solely to variability in n .

The ORCHIDEE GPP sensitivity analysis. The ORCHIDEE land surface model (CMIP6 version)^{31,32}, which is the terrestrial part of the IPSL (Institute Pierre-Simon Laplace) Earth system model, was used to explore the sensitivity of modelled GPP to uncertainty in a wide range of parameters. ORCHIDEE relies on the van Genuchten model to calculate Ψ_s , as well as the hydraulic conductivity and diffusivity required to solve the Richard’s diffusion equation. ORCHIDEE discretizes the first 2 m of the soil column over 11 layers. For this experiment, we ran ORCHIDEE over three single-mesh locations using local half-hourly forcing data to drive the model at each site (Supplementary Table 3) and considered modelled GPP at a daily time step. The sensitivity analysis results shown in Fig. 3 were generated using Sobol’s method³⁰, using the SALib python package⁸⁷ to sample the parameter space and execute the algorithms. Briefly, the model was run using different parameter ensembles, with parameters varied within their reported ranges of uncertainty. Then, each modelled GPP time series was compared with GPP derived from flux-tower observations. The variance of simulated GPP was then decomposed into fractions that can be attributed to each parameter tested. These results, shown in Fig. 3, capture both independent and interactive contributions of each parameter to the total variance. When interactions are removed, the independent contribution of water-retention-curve parameters is still significant, and actually increases for the semi-arid site (see details in Supplementary Information section 3).

The AmeriFlux GPP analysis. Half-hourly or hourly data from the four flux towers referenced in Fig. 4 were acquired from the AmeriFlux network (ameriflux.lbl.gov) and subjected to standardized quality-control, gap-filling, and partitioning approaches. The sites and quality-control procedures are described in more detail in Supplementary Table 5. The methods used to determine the relationship between GPP and soil moisture are similar to those previously used to explore the relationship between surface conductance and soil moisture³⁵. Briefly, analysis was constrained to the peak of the growing season to limit bias linked to phenological variation in leaf area index. Estimates of Ψ_s for each site were determined from

site-specific water-retention curves^{88,81–83}. The data were then sorted into eight bins representing the 15th, 30th, 45th, 60th, 70th, 80th, 90th and 100th quantiles of the observed values of soil moisture content in each site. Within each bin, data were constrained to relatively high light (net radiation $>300 \text{ W m}^{-2}$) conditions with VPD limited to $1 \leq \text{VPD} \leq 1.5 \text{ kPa}$ in US-MMS, US-TON and US-MOz and $1.5 \leq \text{VPD} \leq 2 \text{ kPa}$ in the more arid US-SRM site. The mean GPP, Ψ_s and θ were then calculated for each bin using the filtered data and normalized by the maximum bin-averaged value observed at each site.

Data availability

The FLUXNET tower data appearing in Fig. 3 are from the FLUXNET 2015 dataset (<https://doi.org/10.18140/FLX/1440186> for SD-Dem, <https://doi.org/10.18140/FLX/1440071> for US-HA1 and <https://doi.org/10.18140/FLX/1440160> for FI-SOD). The AmeriFlux tower data appearing in Fig. 4 are available from the AmeriFlux network (<https://doi.org/10.17190/AMF/1246080> for US-MMS, <https://doi.org/10.17190/AMF/1246081> for US-MOz, <https://doi.org/10.17190/AMF/1246104> for US-SRM and <https://doi.org/10.17190/AMF/1245971> for US-TON).

Code availability

The HYDRUS 1D programme used to create the results of Fig. 2e–g is available for public download from <https://www.pc-progress.com/en/Default.aspx?hydrus-1d>. A reference version of the ORCHIDEE land-surface model, used for Fig. 3, is available at <https://orchidee.ipsl.fr/>. Details on the parameterizations of these models are presented in the Supplementary Information.

References

87. Herman, J. & Usher, W. SALib: an open-source Python library for sensitivity analysis. *J. Open Source Softw.* <https://doi.org/10.21105/joss.00097> (2017).

Acknowledgements

K.A.N. acknowledges support from NSF (DEB, grant 1552747) and the AmeriFlux Management Project via the US Department of Energy, Office of Science Lawrence Berkeley National Laboratory. A.G.K. was supported by NASA Terrestrial Ecology (award 80NSSC18K0715). J.D.W. acknowledges support from the US Department of Energy, Office of Science, through Oak Ridge National Laboratory’s Terrestrial Ecosystem Science Focus Area. K.J.D. and Y.S. were supported by National Science Foundation grant EAR 1331726 (S. Brantley) for the Susquehanna Shale Hills Critical Zone Observatory.

Author contributions

K.A.N. conceived of the study with substantial input from D.L.F., A.G.K., K.J.D., T.A.G., R.L.S., B.N.S., Y.S. and N.M. Data analyses were performed by K.A.N., T.A.G., D.L.F. and N.R., who also created the resulting figures. D.B., R.L.S., K.A.N. and J.D.W. contributed AmeriFlux data used in Fig. 4. All authors wrote the text and provided substantial conceptual input to the manuscript.

Competing interests

The authors declare no competing interests.

Additional information

Supplementary information The online version contains supplementary material available at <https://doi.org/10.1038/s41561-022-00909-2>.

Correspondence should be addressed to Kimberly A. Novick.

Peer review information *Nature Geoscience* thanks Christopher Still, Vincent Humphrey and the other, anonymous, reviewer(s) for their contribution to the peer review of this work.

Reprints and permissions information is available at www.nature.com/reprints.